WOOD RESEARCH
58 (4): 2013
533-542

PREPARATION OF WOODEN ACTIVATED CARBON FIBERS USING DIFFERENT STEAM FLOW

Wenjing Liu, Guangjie Zhao
Beijing Forestry University, College of Material Science and Technology
Beijing, China

(Received November 2012)

ABSTRACT

To make better use of wooden resources, activated carbon fibers were prepared from liquefied wood. The influence of activation and steam flow on microstructure and performance of the liquefied wooden carbon fibers (LWCFs) and activated carbon fibers (LWACFs) were investigated. It was founded that the activation resulted in numerous by-products emitted and the damage to graphite-like structure of LWCFs. As the steam flow decreased, the activation was strengthened. Therefore, at higher steam flow, the yield increased and the samples' surface was etched. Their specific surface area, pore volume, and micropore width were also directly related to the steam flow. The specific surface area of LWACFs was as large as that of the commercial activated carbon fiber. The range of their total pore volume was 0.644-0.769 $cm^3.g^{-1}$ which is larger than that of the PAN-ACF and rayon-based ACF. Furthermore, with an increase in steam flow, the quantity of element C increased, while the quantity of element O decreased. Meanwhile, as the steam flow level became higher, the relative content of graphitic carbon and –COOH groups decreased, whereas that of C-O and carbonate groups increased.

KEYWORDS: Activated carbon fiber, wood, microstructure, performance, liquefaction.

INTRODUCTION

Activated carbon fibers (ACFs) as one kind of highly effective fibrous adsorbent have been successfully applied in many fields, where they are used for the catalyst support, the recovery of organic solvent, the treatment of organic and inorganic waste gases, air cleaning, water purification, medical adsorbents, and electronic material. They are characterized by extensive surface area, high adsorption capacity and adsorption/desorption rates, microporous structure, and special surface reactivity (Chiang et al. 2007).

Polyacrylonitrile (PAN) fibers, pitch fibers, phenolic fibers, cellulose fibers, and lignin fibers are commonly used as the raw materials for preparing ACFs (Xu et al. 2006). As the petrochemical resource's shortage and the environmental pollution are becoming a more serious problem, the

study of wooden ACFs has attracted more attention. Su et al. have prepared the cellulose-based ACFs activated by different temperatures and activators (Su et al. 2012). Uraki et al. have studied the ACFs with large specific surface area from softwood acetic acid lignin (Uraki et al. 2001, 2002). Shen et al. have systematically investigated the pore size and properties of lignin-based activated carbon fibers (Shen et al. 2011). However, in these studies, some component of wood must be separated and wood utilization was lower. Through phenol liquefaction, wood components (cellulose, hemicellulose and lignin) are converted into low molecular weight compounds with high reactivity and a large number of phenolic compounds and non-reactive phenol are produced. The liquefied products become novolac by adding hexamethylenetetramine and then are used to spin fibers. As previously reported, the liquefied wood has been prepared the liquefied wood carbon fibers (LWCFs, Okabe et al. 2005; Ma and Zhao 2010) and liquefied wood activated carbon fibers (LWACFs, Liu and Zhao 2012).

The previous work has suggested that the activation temperature and time have great influence on the microstructure and surface functional groups of liquefied wood activated carbon fibers (Liu and Zhao 2012). As is well known, steam flow is other important influence factor on the performance and structure of activated carbon fibers, and its effect on the LWACFs has been not researched. Therefore, the objectives of this study were to prepare activated carbon fibers with different steam flows and characterize them through the examination of the surface morphology, crystal structure, pore structure and surface functional groups. To study activation mechanism of LWACFs, the structural and chemical differences between LWCFs and LWACFs were also investigated.

MATERIAL AND METHODS

Preparation of LWACFs

The 60-mesh wood flour (*Cunninghamia lanceolata*) was mixed with phenol containing 10 wt % H_3PO_4 as a reaction catalyst. The wood/phenol ratio was 1/5 by weight. The mixture was liquefied by mean of stirring at 160°C for 2.5 h. After the liquefaction of the wood, 5 wt % hexamethylenetetramine, as a synthesis agent, was added to the liquefied wood, all of which was then heated to 170°C in a period of 40 min and held for 10 min to prepare the spinning solution.

The as-spun fibers were prepared by means of fusion spinning at 120°C with the laboratory spinning apparatus. When the fusion spinning was completed, the as-spun fibers were cured via soaking in an acid solution with HCHO and HCl (1:1 by volume) as the main components at 85°C for 2 h to produce precursors. The precursors were then washed with deionized water and finally dried at 90°C for 4 h.

The precursors were heat-treated up to 800°C with a heating rate of 3°C.min^{-1} under the protection of nitrogen. Thereafter these fibers were held at this temperature for 60 min by introducing nitrogen or a steam flow to prepare LWCFs or LWACFs, respectively. In the activation process, the steam flow was varied as shown in Tab. 1. Finally, the yield (wt %) of LWACFs was estimated from the following equation and recorded in Tab.1:

$$\text{Yield} = (w_1\text{-}w_2)/\, w_2 \times 100 \;\rightarrow\; w_1/\, w_2 \times 100$$

where: w_1 and w_2 - the weight of activated carbon fibers and weight of the precursor fibers, respectively.

Tab. 1: The parameter of activation and the yield of sample.

Sample	ACF-1.0	ACF-1.5	ACF-2.0	ACF-2.5
Steam flow (ml/min/g)	1.0	1.5	2.0	2.5
Yield (wt %)	40.7	36.5	35.4	32.0

Characterizations

Scanning electron microscope (SEM)

Surface morphologies of LWACFs were observed by scanning electron microscope (SEM, S-3000N, Hitachi, Japan) using gold-coated samples.

X-ray diffraction analysis (XRD)

The diffraction angle (2θ) was obtained by X-ray diffraction (SHIMADZU, XRD-6000) analysis using CuKa radiation (wavelength 0.154 nm) at 40 kV and 30 mA. Layer distance (d) was determined from the Bragg equation: $\lambda=2d_{002}\sin\theta$. Finally, lattice size (L) was calculated using the Scherrer equation: $L=k\lambda/\beta\cos\theta$ (k is 0.89 for Lc, and 1.84 for La) by substituting a half width of amplitude (β) into this formula (Ma and Zhao 2010).

Nitrogen adsorption-desorption isotherms

A Surface Area Analyzer and a Pore Size Analyzer (Autosorb-iQ_Quantachrome Instr. Co. USA) was used to determine the characteristic data of the BET specific surface area, pore volume, pore size, pore radius, and fractal dimension according to nitrogen adsorption-desorption isotherms. Prior to each measurement, the samples were degassed at 300˚C for 3 h. The specific surface area was calculated by the BET equation. The micropore volume and micropore area were estimated using the micropore method of t-plot. The pore volume and radius were based on the assumption that nitrogen filled the sample pores at a relative pressure of 0.995. The pore size distribution was determined by the density functional theory (DFT). The fractal dimension (D), a measure of roughness of surface, was calculated by the FHH (Frenkel-Halsey-Hill) equation.

X-ray photoelectron spectroscopy (XPS)

The binding energies of various elements (at % of C, O and N) were obtained using an Electron Spectroscopy for chemical analysis system (Thermo Scientific ESCALAB 250Xi). A monochromatic AlKα X-ray (1486.6 eV) source was used for this analysis. The survey scans were collected from the binding energy of 0–1350 eV. The peak fitting was repeated until an acceptable fit was obtained. The positions of deconvoluted peaks were determined based on both literature date and empirically derived values.

RESULTS AND DISCUSSION

Exterior surface

SEM micrographs of samples are presented in Fig. 1. The diameter of precursor is much larger than other fibers due to the carbonization at high temperature. Although the surface of precursor, CF, and ACF-1.0 is smooth, a considerable amount of holes are observed on the surface of the samples of ACF-1.5, ACF-2.0 and ACF-2.5. The results reveal that activation effect on the fibers could be strengthened with an increase in steam flow that was acting as an etchant (Brasquet et al. 2000). Higher steam flow resulted in more etching, thus more holes were formed

by destruction of the walls between some pores (Mangun et al. 2001).

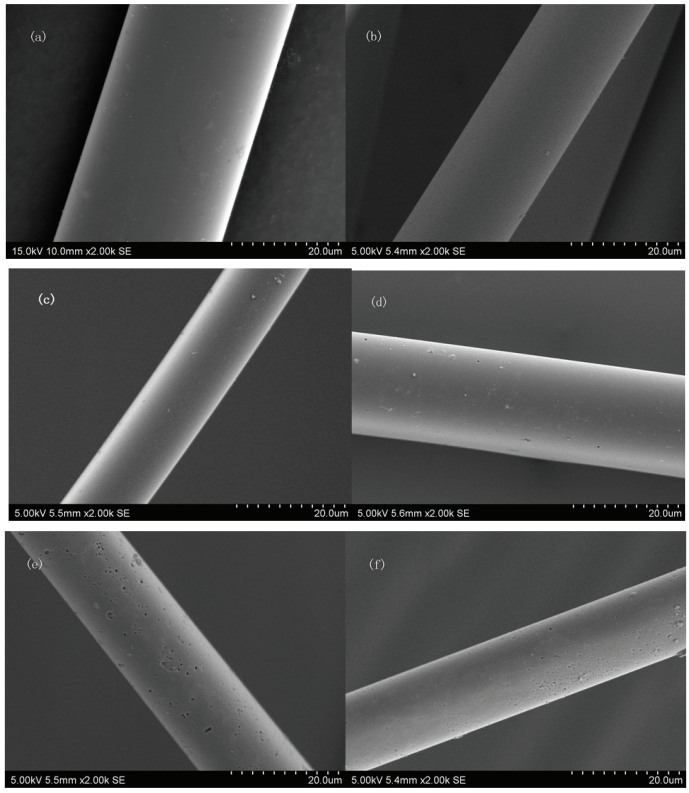

Fig. 1: SEM images of samples: a) Precursor, b) CF, c) ACF-1.0, d) ACF-1.5, e) ACF-2.0, and f) ACF-2.5.

Crystal structure

Fig. 2 shows the X-ray diffraction (XRD) patterns. Two broad peaks are observed to the diffraction angles 2θ at 18-25° and 44°, which are assigned to the disordered graphitic 002 plane and 10 plane (overlapped 100 and 101), respectively (Ryu et al. 2002). There is much difference in the location of 002 peaks for precursors, CFs and ACFs. The 002 peaks of precursors are located in 18° while those of CFs and ACFs are distributed in 25° and 23°, respectively. The 10 peak of precursors is very tiny. These imply that the aromatic structure of precursors was changed gradually into the graphite structure by carbonization and the reaction of activation mainly impacted on 002 peaks. There is little influence on the XRD patterns of ACFs prepared by different steam flows.

The specific graphite-like structural parameters for CFs and ACFs investigated are given in Tab. 2. Generally speaking, the value of the interlayer spacing (d) is inversely related to the degree of graphitization of the carbon materials. A larger stacking height (Lc) and width (La) suggest a larger crystal size, and a higher average carbon layer (Lc/d) further implies a denser structure. Tab. 2 presents the value of d is between 0.3558 nm and 0.3965 nm, which is much

higher than ideal graphite spacing (0.335 nm) would be, demonstrating that all the samples were far from having a graphitized structure. Compared to the graphite-like structural parameters of ACFs, d for CFs is smaller while Lc and Lc/d are larger, indicating that activation reduced the degree of graphitization and stacking height, and the graphite-like structure became loose. In addition, with the increase of the steam flow, the d of ACFs enlarge and the Lc, La, and Lc/d follow an decreasing trend, which suggest that as the steam flow raised, the activation reaction was accelerated, leading to more seriously damage to the graphite-like structure.

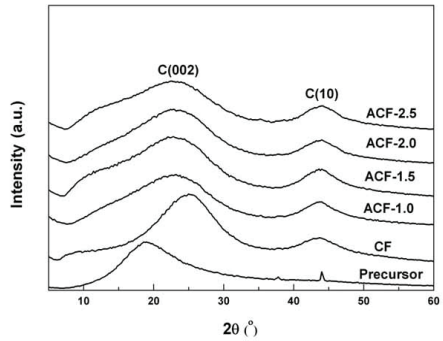

Fig. 2: X-ray diffraction patterns.

Tab. 2: The graphite-like structural parameters.

Samples	d_{002} (nm)	Lc (nm)	La (nm)	Lc/ d_{002}
CF	0.3558	1.0066	3.7210	2.8262
ACF-1.0	0.3830	0.7289	3.9803	1.9032
ACF-1.5	0.3896	0.5935	3.8918	1.5233
ACF-2.0	0.3930	0.5933	3.7262	1.5095
ACF-2.5	0.3965	0.5522	3.5026	1.3927

Pore structure

The nitrogen adsorption-desorption isotherms of the LWACFs with different steam flows are shown in Fig. 3. According to the IUPAC classification, the type of adsorption curve belongs to Type I, which is indicative of the presence of micropores (Chiang et al. 2007). The amount of adsorption increases as the steam flow rises from 1.0 to 2.5 ml/min/g, especially at 2.5 ml/min/g, which illustrates that the total pore volume of the samples increased at higher steam flows. Moreover, at relative pressure of about 0.2, the amount of adsorption still increase with the increase in relative pressure, which reflects a certain volume of mesopores in all the samples (Shen et al. 2005).

Pore characteristics of the LWACFs with different steam flows are summarized in Tab. 3. The table illustrates that the specific surface area (S_{BET}, S_{micro}, and S_{meso}) and pore volume (V_{total}, V_{micro}, and V_{meso}) of the LWACF samples increase with an increase in steam flow. Essentially, these changes are not evident at the flows between 1.0 and 2.0 ml/min/g. However, S_{BET}, S_{micro}, V_{total}, and V_{micro} of sample prepared at the steam flow of 2.5 ml/min/g are much larger than those of other samples. This reflects that numerous pores could be developed at the steam flow of 2.5 ml/min/g due to the serious damage to the graphite-like structure, referring to the results

of XRD analysis. The BET specific surface area of samples varies from 1200 to 1500 $m^2.g^{-1}$. According to previous research, the surface area of pitch-based ACF is approximately 1000 $m^2.g^{-1}$, and that of PAN-ACF and rayon-based ACF is about 1500 $m^2.g^{-1}$ (Chiang et al. 2007; Ishii et al. 1997). The range of total pore volume for those samples is 0.644-0.769 cm^3g^{-1} which is larger than that of the PAN-ACF and rayon-based ACF (0.5-0.6 $cm^3.g^{-1}$, Chiang et al. 2007). As for the pore volume distribution, it is almost not affected by the increase in the steam flow, indicating that micropores and mesopores were both developed at the same rate with the flow ranged from 1.0 to 2.5 ml/min/g. The table also lists that the average pore radius of all samples is approximately 1 nm. The fractal dimension values of the LWACF samples are about 2.6 for D_1, 2.8 for D_2 that are close to 3, demonstrating that their surface were very rough. The different steam flows have little influence on the fractal dimensions. Moreover, it can be also concluded that the fractal dimensions are inversely related to the micropore distribution. This reason was that more pores could lead to a rougher surface.

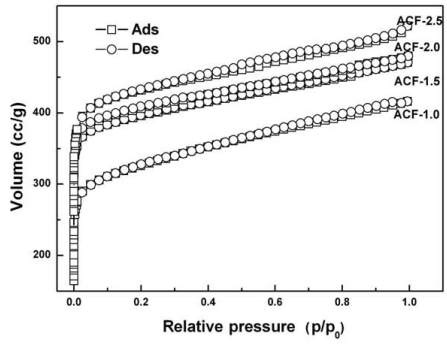

Fig. 3: Nitrogen adsorption-desorption isotherms of the LWACFs.

Tab. 3: Pore characteristics of the LWACF samples.

Sample	Specific surface area ($m^2.g^{-1}$)			Pore volume ($cm^3.g.^1$)			Pore volume distribution (%)		Average pore radius (nm)	Fractal dimensions	
	S_{BET}	S_{micro}	S_{meso}	V_{total}	V_{micro}	V_{meso}	V_{micro}/V_{total}	V_{meso}/V_{total}	r	D_1[a]	D_2[b]
ACF-1.0	1249.511	968.492	281.019	0.644	0.384	0.260	59.627	40.373	1.031	2.606	2.869
ACF-1.5	1252.995	965.646	287.349	0.660	0.388	0.272	58.788	41.212	1.060	2.604	2.868
ACF-2.0	1288.305	990.849	297.456	0.680	0.395	0.285	58.088	41.912	1.055	2.602	2.867
ACF-2.5	1421.515	1126.472	295.043	0.769	0.451	0.318	58.648	41.352	1.082	2.641	2.880

a: $D_1$was obtained by neglecting adsorbate surface tension effects.

b: $D_2$was obtained by accounting for adsorbate surface tension effects.

As shown in Fig. 4, the pore size distributions of the LWACF samples are mainly located between 0.5 and 1.5 nm. As the steam flow raised, the pore volume of samples in 0.5-0.75 nm generally decreased, while that in 0.75-1.5 nm increased. This reflects that the micropore width

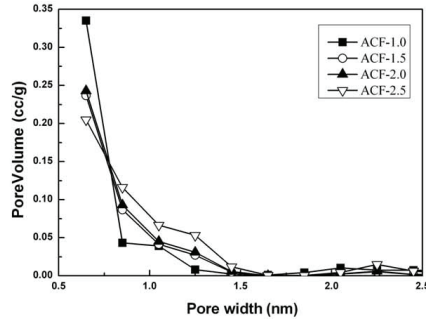

Fig. 4: Pore size distributions of the LWACF samples.

was enlarged with the increase of steam flow. This can be explained by the increase in the interlayer spacing and the damage of micropore walls in the higher steam flows. When the flow rose to 2.5 ml/min/g, there was a slight peak at the pore width of 2.0 to 2.5 nm. This indicates that more mesopores were produced owing to further enlargement of micropore width.

Surface functional groups

The main elemental composition of the surface of the samples is shown in Tab. 4. As seen from the table, elements C and O are their basic elements and element C is the most abundant constituent of all of samples. Comparing the surface elemental composition of all samples, it was found that the carbon fiber samples possessed fewer elements C and more elements O and N. As the steam flow increased, the activated carbon fibers were taken on more elements C and less elements O. The results indicate that elements O were removed by the activation from the samples' surface and their quantity was enlarged at higher steam flow, which can be justified by the analysis of surface functional group.

Tab. 4: Elemental composition of the surface of samples (at %).

Sample	C1s	O1s	N1s	(O)/(C)(%)	(N)/(C) (%)
CF	81.61	17.32	1.07	21.22	1.31
ACF-1.0	90.79	8.89	0.32	9.79	0.35
ACF-1.5	90.70	8.97	0.33	9.99	0.36
ACF-2.0	90.94	8.71	0.36	9.58	0.39
ACF-2.5	92.31	7.36	0.33	7.97	0.36

In order to obtain information about the chemical composition of the fiber surface and the binding characteristics of the elements at the surface, measurements of the XPS spectra of the C1s region were analyzed. The C1s spectra of the four samples are almost the same, thus only the ACF-1.0 sample is shown in Fig. 5 as an example. In the figure, the spectra of C1s region exhibited an asymmetric tailing, which was partially due to the intrinsic asymmetry of the graphite peak or to the contribution of oxygen surface complexes. Curve fitting was optimized into five peaks: the graphitic carbon (BE = 284.7~284.8 eV), carbon present in phenolic, alcohol, ether or C = N groups (BE = 285.5~286.4 eV), carbonyl or quinine groups (BE = 286.8~288.1eV), carboxyl or ester groups (BE = 288.8-289.3 eV), and carbonate groups (BE = 290.8-291.1 eV) (Chiang et al. 2007).

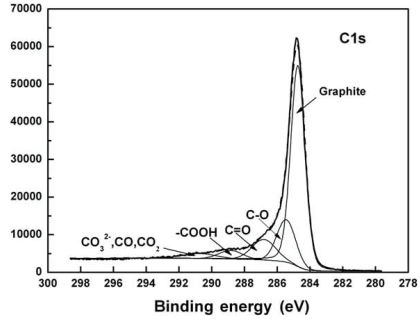

Fig. 5: XPS spectra of C1s region.

The results of the fits of the C1s region are listed in Tab. 5. It can be seen in the table that the relative content of the graphitic carbon decrease as the steam flow increases. It is believed that more graphitic carbon could react with steam molecules to generate the carbon bonded to oxygen-containing functions when the steam flow increased. Aside from the graphitic carbon, C-O groups were the predominant function on the surface samples. The relative composition of the fibers' surface is similar to that of published data (Paiva et al. 2000; Park et al. 2003). In addition, the relative content of C-O, C=O, and carbonate groups was generally in positive correlation with steam flow, which can be attributed to more graphitic carbon transformed at higher steam flow. However, with increasing steam flow, the relative content of –COOH groups decreased, indicating that these carbon bonded to oxygen-containing functions could interact with each other or steam molecules and some by-products released from the surface as the form of CO_2, CO or H_2O. Meanwhile, the activation reaction was accelerated and more by-products were released from the samples with the increase of steam flow (Ma et al. 2005). Therefore, the weight loss increased and elements O decreased with the increase in steam flow.

Tab. 5: Results of the fits of the C1s region.

Sample	Graphite		C-O		C=O		-COOH		CO_3^{2-},CO,CO_2	
	BE (eV)	Relative percentage (%)	BE (eV)	Relative percentage (%)	BE (eV)	Relative percentage (%)	BE (eV)	Relative percentage (%)	BE (eV)	Relative percentage (%)
CF	284.8	66.94	286.4	14.47	288.1	7.63	289.3	4.40	291.1	6.55
ACF-1.0	284.7	64.11	285.5	14.89	286.9	9.88	289.1	5.91	291.4	5.21
ACF-1.5	284.7	62.99	285.7	15.02	287.0	8.45	289.0	5.59	291.1	7.95
ACF-2.0	284.7	61.84	285.6	15.26	286.9	9.80	289.0	5.33	291.0	7.77
ACF-2.5	284.7	61.89	285.5	15.54	286.8	9.99	288.8	4.47	290.7	8.10

CONCLUSIONS

The LWACFs were prepared from liquefied wood through steam activation with different steam flows. The burn-off value of LWACF samples increased gradually with the increase of the steam flow. A certain amount of holes were formed at higher steam flows judging from the SEM images.

In general, as steam flow rose, d increased while Lc, La, and Lc/d decreased. These

suggested that the activation reaction was accelerated at higher steam flow, leading to the damage of graphite-like structure more seriously.

The nitrogen adsorption-desorption isotherms belonged to Type I. This indicated the presence of micropores. The specific surface area (S_{BET}, S_{micro}, and S_{meso}) and pore volume (V_{total}, V_{micro}, and V_{meso}) of the LWACF samples increased with the increase in the steam flow. In addition, the width of micropores and the quantity of mesopores both increased as the steam flow increased. The fractal dimensions value of all of the LWACF samples were close to 3, indicating that their surfaces were very rough. The different treatments had little influence on the fractal dimensions.

The element C was the most abundant constituent of all the LWACFs. As the steam flow increased, the amount of element C increased while that of element O decreased. Meanwhile, as the steam flow level became higher, the relative content of graphitic carbon and –COOH groups decreased and that of C-O and carbonate groups increased. In addition, the C-O groups were the predominant function on the surface of LWACFs.

ACKNOWLEGMENT

The authors are grateful for the support of the Special Research Funds of Forestry Industry for Public Welfare of China, Grant. No. 201004057.

REFERENCES

1. Brasquet, C., Rousseau, B., Estrade-Szwarckopf, H., Le Cloirec, P., 2000: Observation of activated carbon fibres with SEM and AFM correlation with adsorption data in aqueous solution. Carbon 38(3): 407-422.
2. Chiang, Y.C., Lee, C.C., Lee, H.C., 2007: Characterization of microstructure and surface properties of heat-treated PAN-and rayon-based activated carbon fibers. Journal of Porous Materials 14(2): 227-237.
3. Ishii, C., Suzuki, T., Shindo, N., Kaneko, K., 1997: Structural characterization of heat-treated activated carbon fibers. Journal of Porous Materials 4(3): 181-186.
4. Liu, W., Zhao, G., 2012: Effect of temperature and time on microstructure and surface functional groups of activated carbon fibers prepared from liquefied wood. Bioresources 7(4): 5552-5567.
5. Ma, X., Zhao, G., 2010: Preparation of carbon fibers from liquefied wood. Wood Science and Technology 44(1): 3-11.
6. Ma, X., Zhang, L., Peng, J., Zhang, S., Tu, J., Fan, X., Guo, S., 2005: Study on preparing of activated carbon from walnut shells by water vapor. Gold 26(6): 36-40.
7. Mangun, C.L., Benak, K.R., Economy, J., Foster, K.L., 2001: Surface chemistry, pore sizes and adsorption properties of activated carbon fibers and precursors treated with ammonia. Carbon 39(12): 1809-1820.
8. Okabe, K., Yao, T., Shiraishi, N., Oya, A., 2005: Preparation of thin carbon fibers from waste wood-derived phenolic resin. Journal of Materials Science 40(14): 3847-3848.

9. Paiva, M.C., Bernardo, C.A., Nardin, M., 2000: Mechanical, surface and interfacial characterisation of pitch and PAN- based carbon fibres. Carbon 38(9): 1323-1337.
10. Park, S.J., Seo, M.K., Lee, Y.S., 2003: Surface characteristics of fluorine-modified PAN-based carbon fibers. Carbon 41(4): 723-730.
11. Ryu, Z.Y., Rong, H.Q., Zheng, J.T., Wang, M.Z., Zhang, B.J., 2002: Microstructure and chemical analysis of PAN-based activated carbon fibers prepared by different activation methods. Carbon 40(7): 1144-1147.
12. Shen, Q., Zhang, T., Zhang, W.X., Chen, S., Mezgebe, M., 2011: Lignin-based activated carbon fibers and controllable pore size and properties. Journal of Applied Polymer Science 121(2): 989-994.
13. Shen, W., Zheng, J.T., Guo, Q.J., 2005: Preparation of high surface area mesoporous activated carbon fiber and its adsorption properties of sulfides from light oil. Studies in surface Science and Catalysis 156: 951-956.
14. Su, C., Zeng, Z.L., Peng, C.C., Lu, C.H., 2012: Effect of temperature and activators on the characteristics of activated carbon fibers prepared from viscose-rayon knitted fabrics. Fibers and Polymers 13(1): 21-27.
15. Uraki, Y., Kubo, S., Sano, Y., 2002: Preparation of activated carbon moldings from the mixture of waste newspaper and isolated lignins: Mechanical strength of thin sheet and adsorption property. Journal of Wood Science 48(6): 521-526.
16. Uraki, Y., Nakatani, A., Kubo, S., Sano, Y., 2001: Preparation of activated carbon fibers with large specific surface area from softwood acetic acid lignin. Journal of Wood Science 47(6): 465-469.
17. Xu, B., Wu, F., Cao, G., Yang, Y., 2006: Effect of carbonization temperature on microstructure of PAN-based activated carbon fibers prepared by CO_2 activation. New carbon materials 21(1): 1-5.

Wenjing Liu, Guangjie Zhao
Beijing Forestry University
College of Material Science and Technology
Qinghua Eastroad 35
Beijing
China 100083
Phone: 86 010 62337751
Corresponding author: wenjing-1999@163.com